PHYSICAL REVIEW D **96,** 036019 (2017)

ρ meson unpolarized generalized parton distributions with a light-front constituent quark model

Bao-Dong Sun[1,2,*] and Yu-Bing Dong[1,2,3]

[1]*Institute of High Energy Physics, Chinese Academy of Sciences, Beijing 100049, People's Republic of China*
[2]*School of Physics, University of Chinese Academy of Sciences, Beijing 100049, People's Republic of China*
[3]*Theoretical Physics Center for Science Facilities (TPCSF), CAS, Beijing 100049, People's Republic of China*

(Received 20 July 2017; published 31 August 2017)

We study ρ meson unpolarized generalized parton distributions based on a light-front constituent quark model where the quark-antiquark-meson vertex is constructed under the symmetric loop momentum convention. The form factors and some other low-energy observables of the ρ meson are calculated. Moreover, the contributions to the form factors and generalized parton distributions from the valence and nonvalence regimes are discussed and analyzed in detail. In the forward limit, the usual structure functions are estimated as well. In addition, by evolving the moments of the obtained structure functions to the scale of the lattice calculation, we give the factorization scale of our quark model. It is found that the present phenomenological model is reasonable to describe the general properties of ρ meson.

DOI: 10.1103/PhysRevD.96.036019

I. INTRODUCTION

It is known that the usual parton distribution functions (PDFs) and electromagnetic form factors (FFs) shed light on the "one-dimensional" structure of hadrons [1]. Moreover, generalized parton distributions (GPDs) naturally embody the information of both PDFs and FFs, and therefore they display the unique properties to present a "3D" description for the transverse and longitudinal partonic degrees of freedom inside the system, and they contain promising potential which gives arise to ideals of "quark/gluon imaging" of hadrons [1]. Many theoretical investigations have been carried out on the general properties of GPDs for a hadronic system [2]. It is believed that the studies of GPDs are closely related to the processes of deeply virtual Compton scattering and the deeply virtual meson electroproduction [3–5]. By comparing with experimental measurements, one can obtain possible constrains on the GPDs of a hadron [6,7]. With the help of sum rules, the unpolarized GPDs are directly connected to the electromagnetic FFs of the system. There are some empirical parameterizations for GPDs. For the nucleon case, those parametrizations can be obtained by fitting the experimental data to the Dirac, Pauli, and axial FFs [8–12]. In the forward limit, GPDs reproduce the usual PDFs, and thus a description of GPDs can also be built with the help of the experimental data of PDFs [11]. In addition, the moments of GPDs can provide other new information as well, such as the neutron asymmetry [13] and the quark orbital angular momentum [14,15].

Many endeavors have been made to study the GPDs of simple hadrons in the literature, like the studies of a pion [4,16–19]; of a proton and neutron [10–12,20–22]; and of the light nuclei, ^{3}He [13,23], or deuteron [8,24–27]. In those works, different approaches have been employed. They include the chiral quark models employing the Nambu–Jona-Lasinio model, the spectral quark model [16,28,29], the covariant constituent quark models (CCQMs) [17,18,30], the Dyson-Schwinger equation approach [19], the AdS/QCD inspired light-front wave functions [22], and some empirical parametrizations as already mentioned above. Among those phenomenological approaches, the light-cone constituent quark model (LCCQM), one of the CCQMs, is a quite suitable and successful approach to be applied for the studies of the quark-hadron vertex and of the hadron properties, as has been pointed out by Refs. [18,31]. Besides the various model-dependent studies, some lattice QCD calculations have been also performed [32,33]. It is believed that those lattice simulations, together with the experimental data, can be employed to check and make a judgement for the different phenomenological models.

Apart from the pion (spin-0) and nucleon (spin-1/2) targets, the deuteron (spin-1) target is also common experimentally. The GPDs of a deuteron have been already defined through the matrix operators on the light front [24], and the partonic structures and FFs of the deuteron have been formally explored through different approaches as well [25–27,34–36]. We know that the deuteron is a weakly bound system of a proton and a neutron and approximately satisfies the isospin symmetry. Therefore, by considering the GPDs of the proton and neutron, one may obtain the information of the deuteron GPDs [8,25,37].

*sunbd@ihep.ac.cn

The ρ meson, which is a spin-1 particle as well, is usually regarded as a $q\bar{q}$ bound state in CCQMs. Some lattice results [38] have already shown that the ρ meson is approximately a pure $^3S_1$ state with only $\sim 1\%$ admixture of the $^3D_1$ wave, and, consequently, in the rest frame, the valence quarks carry out almost completely the spin of the ρ meson. This conclusion provides a solid support to employ the constituent quark model to explore the ρ meson structure as a pure $q\bar{q}$ system. It should be stressed that the most previous studies of the ρ meson focus on its FFs [39–46]. The only one lattice QCD calculation for the moments of the unpolarized ρ meson PDFs appeared two decades ago [47], which was performed at the scale $Q = 2.4$ GeV. With a quenched approximation, Ref. [47] obtained the nth moments of its structure functions, which is meaningful only when comparing with the nonsinglet valence quark distributions. Later on, the result of QCD sum rules for the ρ meson structure functions in Ref. [48] matches the lattice calculation well. As for the ρ GPDs, there are some possible indirect approaches to access them, such as through the connection with generalized distribution amplitudes, via the double distributions [2,49,50] or the Radon transformation [51]. Thus, it is of a great interest to see what the GPDs of the ρ meson look like with the help of the LCCQM model. This study may be even useful to understand the processes involving the ρ meson lepton production such as $e + N \to e + \rho^0 + N$ [7,25,52,53] or the process of $\gamma\gamma* \to \rho\rho$ [54] and the future Electron-Ion Collider (EIC) experiments [55,56].

In analogy to the deuteron case, we introduce the GPDs of the ρ meson and apply the LCCQM for the study of its unpolarized GPDs. Particularly, the GPDs with different skewness ξ will be discussed in detail. It should be mentioned that in the LCCQM, the separation of the valence Dokshitzer-Gribov-Lipatov-Altarelli-Parisi (DGLAP) and nonvalence Efremov-Radyushkin-Brodsky-Lepage (ERBL) regimes is transparent after the integration over the poles in the Dirac propagators of $k^- = k^0 - k^3$, i.e. the minus component of the loop momentum. Consequently, we can further study the contributions to the properties of the ρ meson, like its FFs and GPDs, from the valence and nonvalence regimes at different values of ξ.

This paper is organized as follows. Section II gives a brief introduction to the general decomposition of GPDs for the spin-1 $\times$ ρ meson. Section III shows a description of the LCCQM. Moreover, in Sec. IV, we display the main numerical results for the ρ meson FFs and its unpolarized GPDs with the LCCQM. In addition, in Sec. V, we discuss the QCD evolution of the moments of the ρ meson PDFs and make a comparison to the lattice calculation. Finally, Sec. VI is devoted to a short summary.

II. GPDS FOR HADRONS WITH SPIN 1

The notations in this work are [30]

$$\begin{aligned} &t = \Delta^2 = (p' - p)^2, \\ &\xi = -\frac{\Delta \cdot n}{2P \cdot n} = -\frac{\Delta^+}{2P^+}, \qquad |\xi| = \frac{\Delta^+}{2P^+}, \qquad (|\xi| \le 1) \\ &x = \frac{k \cdot n}{P \cdot n} = \frac{k^+}{P^+}, \qquad (-1 \le x \le 1), \end{aligned} \tag{1}$$

where p and p' are the 4-momenta of the incoming and outgoing ρ mesons, $P = (p' + p)/2$, $\Delta = p' - p$, n is a lightlike 4-vector with $n^2 = 0$, and k is the 4-momentum in the loop which will be specified in next section. The skewness variable ξ plays a similar role as the Bjorken variable [37,57].

The helicity counting rules restrict that there are totally nine helicity conserving GPDs of the spin-1 particle for each quark flavor and the gluons. Five of them are unpolarized (averaged over helicities), and the other four are polarized (sensitive to helicities). The helicity-averaged GPDs are defined through the two-parton correlation function for quarks as [24]

$$\begin{aligned} V_{\lambda'\lambda} &= \frac{1}{2}\int \frac{d\omega}{2\pi} e^{ix(Pz)} \langle p', \lambda' | \bar{q}\left(-\frac{1}{2}z\right) \not{n} q\left(\frac{1}{2}z\right) | p, \lambda \rangle |_{z=\omega n} \\ &= \sum_i \epsilon'^{*\nu} V^{(i)}_{\nu\mu} \epsilon^\mu H^q_i(x, \xi, t), \end{aligned} \tag{2}$$

where $\epsilon = \epsilon(p, \lambda)$ [or $\epsilon' = \epsilon'(p', \lambda')$] and λ(or λ') $= 0, \pm 1$ are the initial (or final) polarization vector and its helicity, respectively. The explicit expressions of ϵ and the helicity amplitudes of the matrix elements were introduced in Ref. [24]. The helicity amplitudes give the connection between GPDs and the Deep Inelastic Scattering (DIS) structure functions by taking the forward limit. It is argued that there are five independent tensor structures that the tensor $V^{(i)}_{\nu\mu}$ in Eq. (2) would explicit depend on,

$$\{g_{\nu\mu}, P_\nu n_\mu, n_\nu P_\mu, P_\nu P_\mu, n_\nu n_\mu\}. \tag{3}$$

Consequently, the GPDs of the ρ meson are defined as

$$\begin{aligned} V_{\lambda'\lambda} = &-(\epsilon'^* \cdot \epsilon) H^q_1 + \frac{(\epsilon \cdot n)(\epsilon'^* \cdot P) + (\epsilon'^* \cdot n)(\epsilon \cdot P)}{P \cdot n} H^q_2 - \frac{2(\epsilon \cdot P)(\epsilon'^* \cdot P)}{M^2} H^q_3 \\ &+ \frac{(\epsilon \cdot n)(\epsilon'^* \cdot P) - (\epsilon'^* \cdot n)(\epsilon \cdot P)}{P \cdot n} H^q_4 + \left\{ M^2 \frac{(\epsilon \cdot n)(\epsilon'^* \cdot n)}{(P \cdot n)^2} + \frac{1}{3}(\epsilon'^* \epsilon) \right\} H^q_5, \end{aligned} \tag{4}$$

where M is the ρ meson mass. The five unpolarized GPDs $H_i^q (i = 1 \sim 5)$ are the functions of x, ξ, and t. The explicit dependence of H_i^q on the three variables is omitted for simplicity.

A. Sum rules

The conventional form factor decomposition of the vector current for a spin-1 particle is

$$\begin{aligned} I^\mu_{\lambda'\lambda} &= \langle p', \lambda' | \bar{q}(0)\gamma^\mu q(0) | p, \lambda \rangle \\ &= \epsilon'^{*\beta}\epsilon^\alpha \left[-\left(G_1^q(t) g_{\beta\alpha} + G_3^q(t) \frac{P_\beta P_\alpha}{2M^2} \right) P^\mu \right. \\ &\quad \left. + G_2^q(t)(g^\mu_\alpha P_\beta + g^\mu_\beta P_\alpha) \right]. \end{aligned} \tag{5}$$

The conventional FFs $G_{1,2,3}$ are obtained from $G^q_{1,2,3}$ by weighting with electromagnetic charges and then summing over flavors: $G_i = e_u G_i^u + e_{\bar{d}} G_i^{\bar{d}}$ for $i = 1, 2, 3$. It is equivalent to using the isospin combination, which will be shown later in Eq. (39). Comparing with Eq. (4), one can obtain the sum rules,

$$\begin{aligned} &\int_{-1}^{1} dx H_i^q(x, \xi, t) = G_i^q(t) \quad (i = 1, 2, 3), \\ &\int_{-1}^{1} dx H_i^q(x, \xi, t) = 0 \quad (i = 4, 5). \end{aligned} \tag{6}$$

The integrals of H_4^q and H_5^q vanish due to the constraints of time reversal and Lorentz invariance, respectively [24].

The FFs $G_{C,M,Q}$ can be expressed in terms of $G_{1,2,3}$ as [42]

$$\begin{aligned} G_C(t) &= G_1(t) + \frac{2}{3}\eta G_Q(t), \\ G_M(t) &= G_2(t), \\ G_Q(t) &= G_1(t) - G_2(t) + (1 + \eta) G_3(t), \end{aligned} \tag{7}$$

where $\eta = -t/4M^2$. Together with Eq. (6), one can obtain $G_{C,M,Q}$ directly from GPDs $H_{1,2,3}$. Note that in many previous studies, the calculation of $G_{C,M,Q}$ from the matrix elements of $I^+_{\lambda'\lambda}$ is faced with the well-known ambiguity of the angular condition [39]. Some different prescriptions are proposed to avoid the "worst" matrix elements. The present work bypasses this ambiguity.

The normalizations take

$$G_C(0) = 1, \qquad G_M(0) = 2M\mu, \qquad G_Q(0) = M^2 Q_\rho, \tag{8}$$

where μ and Q_ρ are the ρ magnetic dipole and quadrupole moments. The mean square charge radius $\langle r^2 \rangle$ is given by

$$\langle r^2 \rangle = \lim_{t \to 0} \frac{6[G_C(t) - 1]}{t}. \tag{9}$$

B. Forward limit

For $x > 0$, the helicity amplitudes in the forward limit ($\Delta = 0$) give the relations between GPDs and the unpolarized (quark-spin-averaged) parton distributions $q^\lambda(x)$ [24,47], with λ being the polarization of the ρ meson, as

$$\begin{aligned} H_1^q(x, 0, 0) &= \frac{q^1(x) + q^{-1}(x) + q^0(x)}{3} = q(x), \\ H_5^q(x, 0, 0) &= q^0(x) - \frac{q^1(x) + q^{-1}(x)}{2}. \end{aligned} \tag{10}$$

For $x < 0$, the above equations with an overall sign change give the antiquark distributions at $-x$. Here, the unpolarized quark density is defined as $q^\lambda = q^\lambda_\uparrow + q^\lambda_\downarrow$, where $\uparrow$ ($\downarrow$) stands for up (down) spin projection along the direction of the motion when the ρ meson moves with infinite momentum. In the constituent quark model, the sum rules, corresponding to the flavor number and momentum conservation, are

$$\int dx u(x) = \int dx \bar{d}(x) = 1, \tag{11}$$

$$\int dx [x(u(x) + \bar{d}(x))] = 1 \tag{12}$$

for the ρ^+ meson.

At leading twist or leading order, the single flavor DIS structure function $F_1^q(x)$ is one-half of the probability to find a quark with momentum fraction x and obeys the Callan-Gross relation [24,47]

$$F_1^q(x) = \frac{1}{3}[q^1_\uparrow(x) + q^1_\downarrow(x) + q^0_\uparrow(x)] = \frac{1}{2} H_1^q(x, 0, 0). \tag{13}$$

The single flavor structure function $b_1^q(x)$, which measures the difference in the spin projection of the ρ meson, only depends on the quark-spin-averaged distribution $q^\lambda(x)$,

$$b_1^q(x) = q^0(x) - \frac{q^1(x) + q^{-1}(x)}{2} = H_5^q(x, 0, 0). \tag{14}$$

From parity, one has $q^\lambda_\uparrow = q^{-\lambda}_\downarrow$, and therefore the conventional structure functions, related to $q^\lambda(x)$, are

$$F_1(x) = \sum_q e_q^2 F_1^q(x), \qquad b_1(x) = \frac{1}{2}\sum_q e_q^2 b_1^q(x). \tag{15}$$

In the following, we will focus on the single flavor structure functions. In the meson case, the structure functions are identical for both flavors. It should be mentioned that the spin-1 particle, different from the spin-1/2 one, has the tensor structure function b_1. It triggers great interest [58–62]. The sum rule of this structure function is $\int dx b_1(x) = 0$ [58].

In addition, the nth Mellin moment of a function $f(x)$ is defined as

$$M_n(f) = \int_0^1 x^{n-1} f(x) dx. \tag{16}$$

For the ρ meson case, to the leading order (twist 2), one finds

$$2M_n(F_1^q) = C_n^{(1)} a_n, \qquad 2M_n(b_1^q) = C_n^{(1)} d_n, \tag{17}$$

where $C_n^{(k)} = 1 + O(\alpha)$ are the Wilson coefficients of the operator product expansion and a_n and d_n are the reduced matrix elements [47]. With the quenched approximation, Ref. [47] found that these relations hold for both even and odd nth orders.

C. Isospin combination

In Eq. (4), GPDs are defined flavor by flavor. Similar to Refs. [29,63], the corresponding isospin projection of the isovector ($I = 1$, nonsinglet) equals

$$\begin{aligned}
&\frac{1}{2}\int \frac{d\omega}{2\pi} e^{ix(Pz)} \langle \rho^b(p',\lambda')|\bar{q}\left(-\frac{1}{2}z\right)\not{n}\tau_3 q\left(\frac{1}{2}z\right)|\rho^a(p,\lambda)\rangle|_{z=\omega n} \\
&= \imath\epsilon_{3ab}\Bigg\{-(\epsilon'^*\epsilon)H_1^{I=1} + \frac{(\epsilon n)(\epsilon'^* P) + (\epsilon'^* n)(\epsilon P)}{Pn} H_2^{I=1} - \frac{2(\epsilon P)(\epsilon'^* P)}{M^2} H_3^{I=1} \\
&\quad + \frac{(\epsilon n)(\epsilon'^* P) - (\epsilon'^* n)(\epsilon P)}{Pn} H_4^{I=1} + \left[M^2 \frac{(\epsilon n)(\epsilon'^* n)}{(Pn)^2} + \frac{1}{3}(\epsilon'^*\epsilon)\right] H_5^{I=1}\Bigg\} \\
&= \imath\epsilon_{3ab}\Bigg\{-(\epsilon'^*\epsilon)(H_1^u - H_1^d) + \frac{(\epsilon n)(\epsilon'^* P) + (\epsilon'^* n)(\epsilon P)}{Pn}(H_2^u - H_2^d) - \frac{2(\epsilon P)(\epsilon'^* P)}{M^2}(H_3^u - H_3^d) \\
&\quad + \frac{(\epsilon n)(\epsilon'^* P) - (\epsilon'^* n)(\epsilon P)}{Pn}(H_4^u - H_4^d) + \left[M^2 \frac{(\epsilon n)(\epsilon'^* n)}{(Pn)^2} + \frac{1}{3}(\epsilon'^*\epsilon)\right](H_5^u - H_5^d)\Bigg\},
\end{aligned} \tag{18}$$

where a, $b = 0$, 1, 2 and $\rho^\pm = \rho^1 \mp \imath\rho^2$. For the isoscalar case ($I = 0$, singlet), one needs the exchange $\not{n}\tau_3 \leftrightarrow \not{n}$, and therefore $H_i^u - H_i^d \leftrightarrow H_i^u + H_i^d$. In the following work, we will only deal with a positive-charged ρ and omit the subscript $+$ whenever no ambiguity arises.

III. OUR APPROACH

In analogy to the chiral interaction Lagrangian for the $\pi \to q\bar{q}$ vertex [64], the effective Lagrangian for the $\rho \to \bar{q}q$ is taken as

$$\begin{aligned}
\mathcal{L}_I &\sim -\imath\frac{M}{f_\rho}\bar{q}\gamma^\mu \boldsymbol{\tau} q \cdot \boldsymbol{\rho}_\mu \\
&= -\imath\frac{M}{f_\rho}[\bar{u}\gamma^\mu u\rho_\mu^0 + \sqrt{2}\bar{u}\gamma^\mu d\rho_\mu^+ + \sqrt{2}\bar{d}\gamma^\mu u\rho_\mu^- + \bar{d}\gamma^\mu d\rho_\mu^0],
\end{aligned} \tag{19}$$

where f_ρ is the ρ decay constant. In the lowest Fock state, the two-parton correlation function, the lhs of Eq. (18), corresponds to a triangle loop [3]. The loop integral, corresponding to the active u quark [see Figs. 1(a) and 2], is specified as

$$\begin{aligned}
V^u(x,\xi,t) = N_{\mu\nu}\int \frac{d^4k}{(2\pi)^4}\delta[n\cdot(xP-k)](-)\mathrm{Tr}\Bigg[&\frac{\imath(\not{k}-\not{P}+m)}{(k-P)^2-m^2+\imath\epsilon}\gamma^\nu \frac{\imath(\not{k}+\frac{\not{\Delta}}{2}+m)}{(k+\frac{\Delta}{2})^2-m^2+\imath\epsilon}\not{n} \\
&\times \frac{\imath(\not{k}-\frac{\not{\Delta}}{2}+m)}{(k-\frac{\Delta}{2})^2-m^2+\imath\epsilon}\gamma^\mu\Bigg]\Lambda(k-P,p')\Lambda(k-P,p),
\end{aligned} \tag{20}$$

where m is the constituent quark mass and

$$N_{\mu\nu} = \frac{M^2}{f_\rho^2}\frac{\epsilon'^*_\nu(p',\lambda')\epsilon_\mu(p,\lambda)}{2(2\pi)^3\sqrt{\omega_{p'}\omega_p}} \tag{21}$$

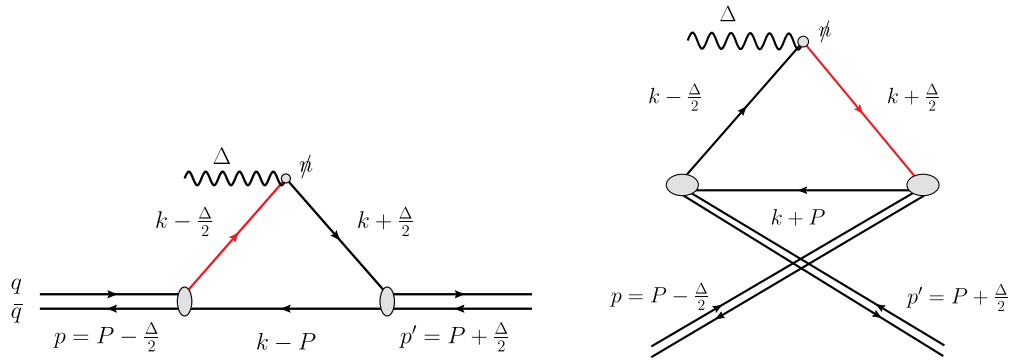

(a)The struck u quark in the valence regime

(b)The struck d quark in the valence regime

FIG. 1. Direct (a) and crossed (b) Feynman diagrams contributing to the GPDs of the quark q and antiquark $\bar{q}$ of the ρ meson. The gray blobs represent the normal Light Front (LF) wave vertexes. The plus component of the momentum carried by red lines has positive sign in the valence regime.

and the scalar function

$$\Lambda(k-P,p)=\frac{c}{[(k-P)^2-m_R^2+\imath\epsilon][(k-\frac{\Delta}{2})^2-m_R^2+\imath\epsilon]} \tag{22}$$

is following Ref. [30], with m_R and c being the regulator mass and the normalization factor, respectively. The loop of the struck d quark can be obtained from the crossed Feynman diagram of Fig. 1(b). Here, the scalar product function $\Lambda(k-P,p)$ is symmetric under the exchange of the momentums of the two constituents. This scalar function is employed to describe the momentum dependence between q and $\bar{q}$ inside the ρ meson. Actually, it plays a role of the momentum cutoff similar to the Pauli-Villars regularization [30]. It may also stand for a property of the Bethe-Salpeter amplitude [65] and contain the information of the nonperturbative effect. Conceptually, by taking $\Lambda(k-P,p)$ as a part of the quark-antiquark-meson vertex, one gets the smeared quark-antiquark-meson vertex, $\gamma^\mu\Lambda(k-P,p)$ [42]. As will be seen later, the symmetric momenta convention, shown in Figs. 1 and 2, enables the vertex to fulfill the constraint from the isospin symmetry.

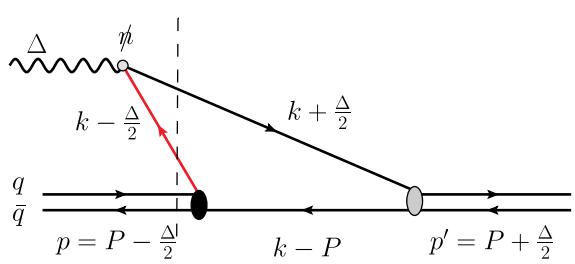

FIG. 2. The struck u quark in the nonvalence regime, yielded by the off-diagonal terms in the Fock space. The black blob represents the non-wave-function vertex. The red line has the negative sign in this regime.

Note that the elastic FFs can be calculated in different reference frames, such as the Drell-Yan frame [31], where $\Delta^+=0$ and $\xi=0$, and the Breit frame, where $\Delta^+=-\Delta^-$ (see Refs. [30,66] for discussions on the motivation of adopting this frame). In this work, the above loop integral is performed in the Breit frame, and then the ξ dependence of GPDs can be obtained as well. In this special reference frame, the momentum transfer and initial and finial momenta are

$$\begin{aligned}\Delta&=(\Delta^+,\Delta^-,\boldsymbol{\Delta}_\perp)=(q_z,-q_z,q_x,q_y),\\ p&=\left(p^0-\frac{q_z}{2},p^0+\frac{q_z}{2},-\frac{\boldsymbol{\Delta}_\perp}{2}\right),\\ p'&=\left(p^0+\frac{q_z}{2},p^0-\frac{q_z}{2},\frac{\boldsymbol{\Delta}_\perp}{2}\right),\end{aligned} \tag{23}$$

where $\boldsymbol{\Delta}_\perp=(q_x,q_y)$ and $p^0=M\sqrt{1-\Delta^2/4M^2}$. Since $\Delta_\perp^2\geq 0$, one gets the constraint $|\xi|\leq 1/\sqrt{1-4M^2/t}$.

The physics in the nonvalence regime, shown in Fig. 2, is remarkably different from the one in the valence regime. According to Ref. [67], the $q\bar{q}$ pair, created by the virtual photon, could interact with itself and form a virtual meson, before merging with the meson state. From another point of view, the higher Fock component contributions should be taken into account in both two regimes for completeness. Instead of finding all higher Fock component contributions as Refs. [68,69], we handle the nonvalence contribution by replacing the simple γ^μ with a phenomenological meson vertex Γ^μ as shown in Ref. [42]. This is an analogy to the covariant form [70], which has been applied for the deuteron case in our previous work [71]. Thus, the smeared quark-antiquark-meson vertex becomes $\Gamma^\mu\Lambda(k-P,p)$.

For the u quark contribution shown in Fig. 1(a), the spectator constituent momentum is $k_s=k_{\bar{d}}=k-P$. The

phenomenological vertices under this loop momentum assignment read

$$\Gamma_i^\mu = \gamma^\mu - \frac{(2k - P - \frac{\Delta}{2})^\mu}{D_i}, \qquad \Gamma_f^\nu = \gamma^\nu - \frac{(2k - P + \frac{\Delta}{2})^\nu}{D_f}, \tag{24}$$

where $D_{i,f} = M_{i,f} + 2m$, and the kinematic invariant masses $M_{i,f}$ are [42]

$$M_i^2 = \frac{\kappa_\perp^2 + m^2}{1 - x'} + \frac{\kappa_\perp^2 + m^2}{x'}, \tag{25}$$

$$M_f^2 = \frac{\kappa_\perp'^2 + m^2}{1 - x''} + \frac{\kappa_\perp'^2 + m^2}{x''}, \tag{26}$$

with the LF momentum fractions $x' = -k_s^+/p^+ = (1-x)/(1-|\xi|)$, $x'' = x'p^+/p'^+ = (1-x)/(1+|\xi|)$, and

$$\kappa_\perp = k_{s\perp} - \frac{k_s^+}{p^+} p_{i\perp} = (k-P)_\perp - \frac{x'}{2}\Delta_\perp,$$
$$\kappa_\perp' = (k-P)_\perp + \frac{x''}{2}\Delta_\perp. \tag{27}$$

In the nonvalence regime, shown in Fig. 2, the relation of $-|\xi| < x < |\xi|$ leads to $x' > 1$, and the initial vertex becomes the non-wave-function vertex. To keep the mass square positive [see M_i in Eq. (25)], Ref. [42] proposes to directly replace $1 - x'$ with $x' - 1$ in Eq. (25) and gets

$$M_{i(NV)}^2 = \frac{\kappa_\perp^2 + m^2}{x' - 1} + \frac{\kappa_\perp^2 + m^2}{x'}. \tag{28}$$

Hereafter, we use the subscripts V and NV to stand for the valence and nonvalence regimes, respectively. Note that, when both the struck and spectator constituents are on mass shells, namely, $(k - \frac{\Delta}{2})^2 = (k-P)^2 = m^2$, one gets $M_i^2 = M_f^2 = M^2$. Due to the exchange $1 - x' \leftrightarrow x' - 1$, the relation of $M_{i(NV)}^2 = M^2$ no longer holds for the nonvalence case. However, M_i^2 and $M_{i(NV)}^2$ have the same limiting value as $x \to |\xi|$, and thus the continuity of GPDs is guaranteed. The physics in the parton-number-changing nonvalence Fock state contributions is much more complicated than that in the valence one, since the creation of the $q\bar{q}$ pair involves an infinite sum of the meson contribution. Due to the lack of the information about the nonvalence regime [67], in some model calculations, the discontinuity may arise at $x = \xi(\text{or}|\xi|)$ where the valence and nonvalence regimes divide, like in Ref. [17] for the π meson GPDs.

With the above preparations, the integral of Eq. (20) in the light-front frame reads

$$\begin{aligned} V^u(x,\xi,t) = N_{\mu\nu} \int \frac{dk^+ dk^- dk_\perp}{4(2\pi)^4} \delta[xP^+ - k^+] \frac{(-)\mathrm{Tr}[\mathcal{O}^{\mu\nu+}]}{(k^+ - P^+)(k^+ + \frac{\Delta^+}{2})(k^+ - \frac{\Delta^+}{2})} \\ \times \frac{1}{[k^- - P^- - (k-P)^-_{on} + i\frac{\epsilon}{k^+ - P^+}]} \frac{1}{[k^- + \frac{\Delta^-}{2} - (k + \frac{\Delta}{2})^-_{\mathrm{on}} + i\frac{\epsilon}{k^+ + \frac{\Delta^+}{2}}]} \\ \times \frac{1}{[k^- - \frac{\Delta^-}{2} - (k - \frac{\Delta}{2})^-_{on} + i\frac{\epsilon}{k^+ - \frac{\Delta^+}{2}}]} \\ \times \Lambda(k-P, p')\Lambda(k-P, p), \end{aligned} \tag{29}$$

where

$$\mathcal{O}^{\mu\nu+} = \imath^3(\not{k} - \not{P} + m)\Gamma_i^\nu \left(\not{k} + \frac{\not{\Delta}}{2} + m\right) \times \gamma^+ \left(\not{k} - \frac{\not{\Delta}}{2} + m\right)\Gamma_f^\mu, \tag{30}$$

$$(k-P)^-_{\mathrm{on}} = \frac{(k-P)_\perp + m^2}{k^+ - P^+}, \text{etc.}, \tag{31}$$

and the Λ functions, Eq. (22), are chosen without changing the distribution of the poles with respect to the three denominators of the propagators. There are six poles with respect to k^- for the integral, the same as in the pion case [30]. They are

$$\begin{aligned} k^-_{1(2)} &= P^- + (k-P)^-_{\mathrm{on}(R)} - i\frac{\epsilon}{k^+ - P^+}, \\ k^-_{3(4)} &= \frac{\Delta^-}{2} + \left(k - \frac{\Delta}{2}\right)^-_{\mathrm{on}(R)} - i\frac{\epsilon}{k^+ - \frac{\Delta^+}{2}}, \\ k^-_{5(6)} &= -\frac{\Delta^-}{2} + \left(k + \frac{\Delta}{2}\right)^-_{\mathrm{on}(R)} - i\frac{\epsilon}{k^+ + \frac{\Delta^+}{2}}, \end{aligned} \tag{32}$$

where $(k-P)^-_R$ and $(k \pm \frac{\Delta}{2})^-_R$ are obtained by replacing m with m_R in Eq. (31), respectively. Since $p'^+ > p^+ > 0$, after integrating over k^-, there are only two regions in k^+ that contribute to the integral, the valence regime $k^+ \in [\Delta^+/2, P^+]$ and the nonvalence one $k^+ \in [-\Delta^+/2, \Delta^+/2]$. In the case $p'^+ = p^+(\xi = 0)$, there is only one regime (valence), and the detail calculation can be found in

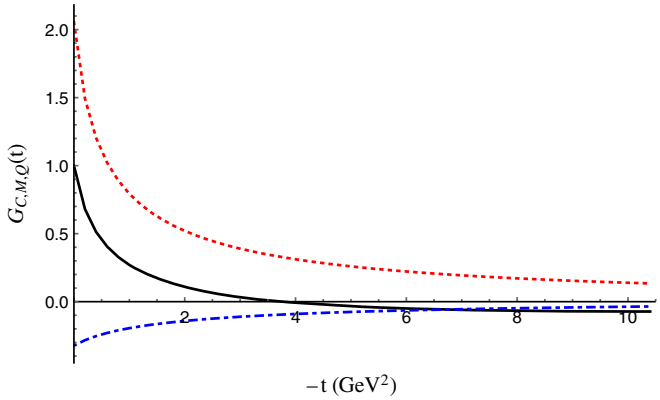

FIG. 3. The ρ FFs, G_C (solid black line), G_M (dashed red line), and G_Q (dot-dashed blue line).

Refs. [64,72]. The first two poles $k^- = k^-_{1(2)}$ contribute to the valence part, and the last two poles $k^- = k^-_{5(6)}$ contribute to the nonvalence one (see Fig. 2). The residue of the pole $k^- = k^-_1$ reads

$$\begin{aligned} V^u_{1(V)}(x,\xi,t) = {} & \frac{-N_{\mu\nu}}{4(2\pi)^4}\int_{\frac{\Delta^+}{2}}^{P^+} dk^+ \int dk_\perp \delta[xP^+ - k^+] \\ & \times \frac{\mathrm{Tr}[\mathcal{O}^{\mu\nu+}]}{(k^+ - P^+)(k^+ + \frac{\Delta^+}{2})(k^+ - \frac{\Delta^+}{2})} \\ & \times \frac{1}{[k^- + \frac{\Delta^-}{2} - (k + \frac{\Delta}{2})^-_{\mathrm{on}} + i\frac{\epsilon}{k^+ + \frac{\Delta^+}{2}}]} \\ & \times \frac{1}{[k^- - \frac{\Delta^-}{2} - (k - \frac{\Delta}{2})^-_{\mathrm{on}} + i\frac{\epsilon}{k^+ - \frac{\Delta^+}{2}}]} \\ & \times \Lambda(k-P,p')\Lambda(k-P,p)|_{k^- = k^-_1}, \end{aligned} \tag{33}$$

and for the rest of the poles, $k^- = k^-_i$, $V^u_{i(V/NV)}(x,\xi,t)$ (i labels different poles) can be obtained similarly. Then, the valence contributions read

$$V^u_{(V)} = V^u_{1(V)} + V^u_{2(V)}, \tag{34}$$

where the ξ-independent (also frame-independent) full result for the u quark GPDs is

$$V^u = V^u_{(V)} + V^u_{(NV)}. \tag{35}$$

It is easy to verify that, under the assignment of loop momenta in Fig. 1, the trace part of the loop integral for the d quark is related to that of the u quark as

$$\mathrm{Tr}[\mathcal{O}^{\mu\nu+}_{(d)}(x,-k)] = -\mathrm{Tr}[\mathcal{O}^{\mu\nu+}(-x,k)]. \tag{36}$$

Therefore, the relation $V^d(x,\xi,t) = -V^u(-x,\xi,t)$ is preserved, as required by the isospin and crossing symmetries [30]. Here, the symmetric momenta convention are essential for the present model to fulfill this constraint. We, thus, get

$$\int_{-1}^{1} dx H^d_i(x,\xi,t) = -\int_{-1}^{1} dx H^u_i(x,\xi,t), \tag{37}$$

with $i = 1 \sim 5$. Finally, the isovector GPDs satisfy

$$H^{I=1}_i(x,\xi,t) = H^{I=1}_i(-x,\xi,t). \tag{38}$$

In addition, from Eq. (6), the sum rules of the conventional FFs, it is easy to see the equivalent [24,29]

$$\begin{aligned} G_i &= e_u \int_{-1}^{1} dx H^u_i(x,\xi,t) + e_d \int_{-1}^{1} dx H^d_i(x,\xi,t) \\ &= \int_{-1}^{1} dx H^{I=1}_i(x,\xi,t). \end{aligned} \tag{39}$$

In our work, the strategy to extract the five GPDs H_i, is to construct five independent equations by replacing $\epsilon'^{*\nu}\epsilon^\mu$ in V^u with the tensors listed in (3) separately and finally to solve them jointly. See the Appendix for more details.

IV. RESULTS

In this work, we take the constituent mass $m = 0.403$ GeV and regulator mass $m_R = 1.61$ GeV. The requirement of stability of the bound states, $m > M/2$ and $m + m_R > M$, is maintained.

The calculated ρ meson FFs and low-energy observables are shown in Fig. 3 and Table I. The nonvalence contributions to FFs $G_{1,2,3}$ at $\xi = -0.2$, -0.4, and -0.6 are shown in Fig. 4. Due to the constraint $|\xi| \le 1/\sqrt{1 - 4M^2/t}$, the corresponding $|t|_{\min}$ are 0.10, 0.45, and 1.33 GeV^2, respectively. Figures 5–7 show the 3D plots of the unpolarized ρ meson GPDs $H_{1,2,3}$ as the functions of variables x and t at the two different skewnesses $\xi = 0$ and -0.4. The values

TABLE I. The ρ meson low-energy observables of the mean square charge radius ($\langle r^2\rangle$), the magnetic dipole (μ), and the quadrupole (Q_ρ) moments in the units of fm^2, $1/2M$, and $1/M^2$, respectively. The results of other LCCQMs [39,40,42,70,73], of the point-form formalism [43], of the lattice QCD [74], and of the experiment measurement [75] are also displayed for a comparison.

	[39]	[40]	[42]	[70]	[73]	[43]	[74]	[75]	this work
$\langle r^2\rangle$	0.37	0.35	⋯	⋯	0.268	⋯	0.670(68)	⋯	0.52
μ	2.14	2.26	1.92	1.83	2.21	2.2	2.613(97)	2.1(5)	2.06
Q_ρ	−0.79	−0.37	−0.43	−0.33	−0.882	−0.47	−0.733(99)	⋯	−0.323

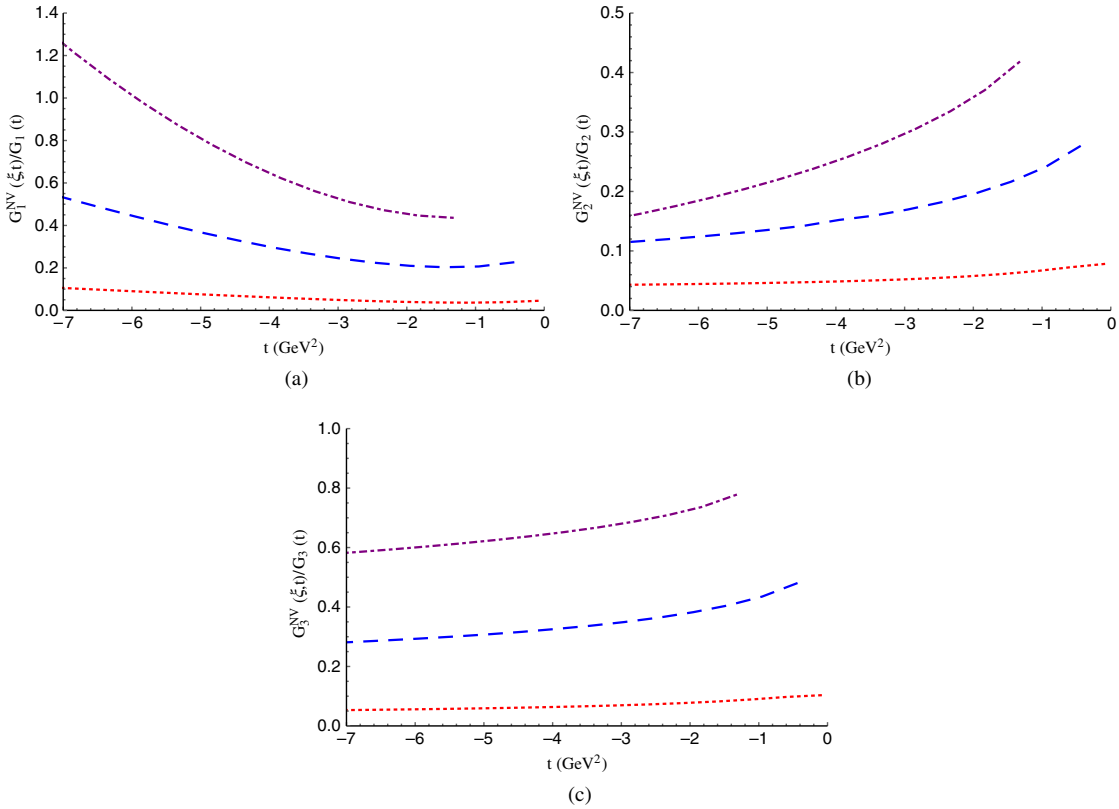

FIG. 4. The nonvalence contributions to FFs G_1, G_2, and G_3 at $\xi = -0.2$ (dotted red line),-0.4 (dashed blue line), and -0.6 (dot-dashed purple line), respectively.

are normalized to the corresponding FFs $G_i(t)$ for a convenience of the comparison. Figures 8–10 show $H_{1,2,3}$ at specific momentum transfers t (-0.5 and -10 GeV^2) and different skewnesses ξ (0, -0.2, -0.4, and -0.6). Due to the symmetry, only the $0 < x < 1$ regime is plotted in Figs. 8–10. Moreover, the two obtained structure functions, $F_1^u(x)$ and $b_1^u(x)$, are plotted in Figs. 11 and 12, respectively.

For the charge form factor G_C in Fig. 3, we found it has a crossing point near $t = -3.8$ GeV^2. Moreover, the tendencies of t dependence of all three obtained FFs agree with the previous results, such as Refs. [40,42,43]. In Table I, other results of the LCCQMs, of the point form, of the lattice QCD, and of the experiment measurement are also listed for a comparison. Although the LCCQM proposed in the present work is inspired by former ones [42,70] (for the

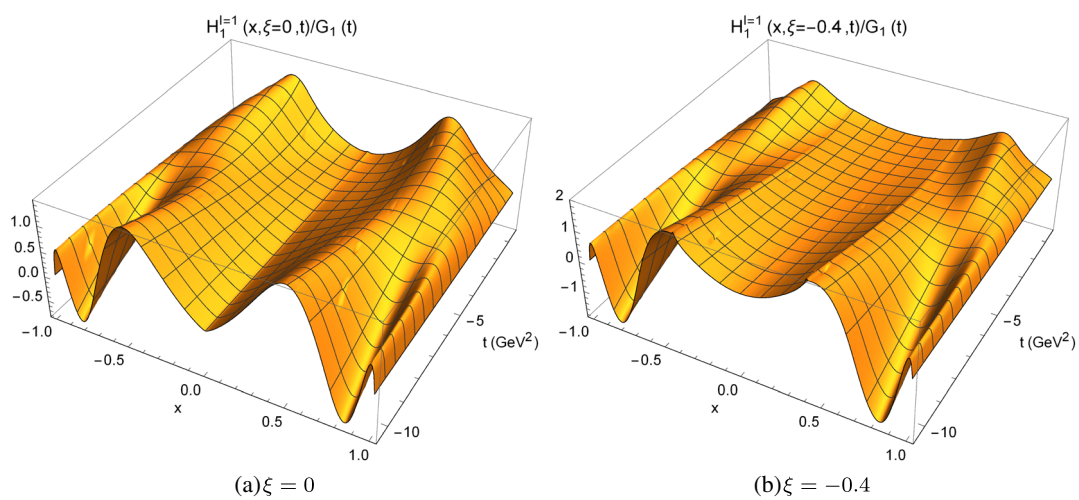

FIG. 5. The 3D ρ^+ GPD H_1 at $\xi = 0$(a) and -0.4(b).

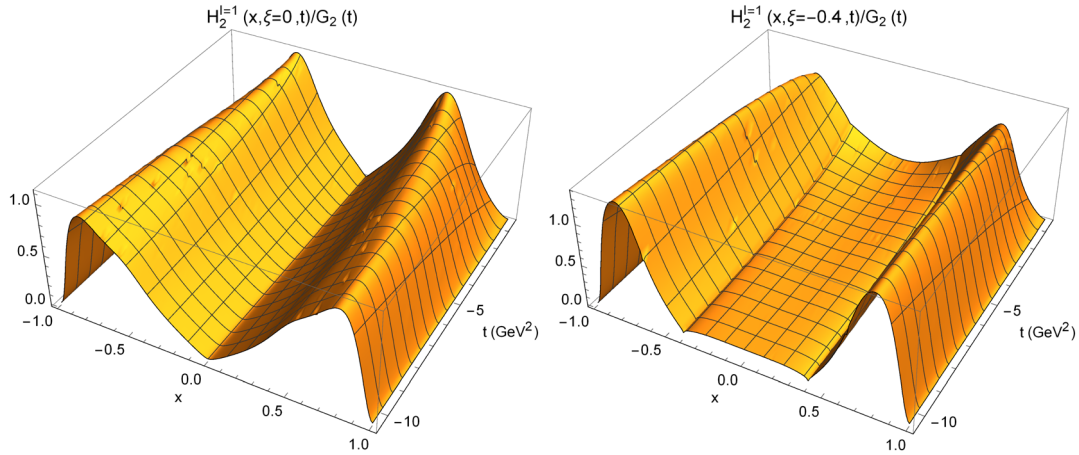

(a) $\xi = 0$ (b) $\xi = -0.4$

FIG. 6. ρ^+ GPD H_2. The same line code is used in Fig. 5.

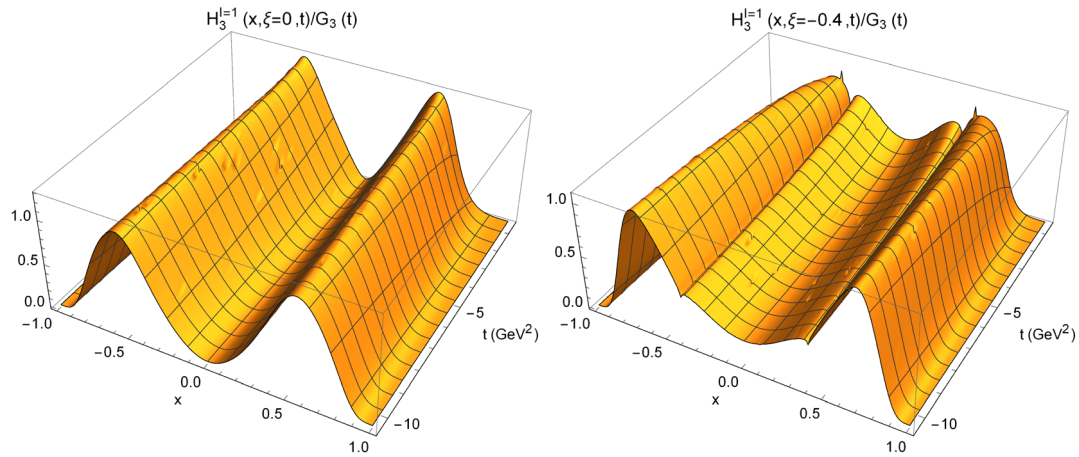

(a) $\xi = 0$ (b) $\xi = -0.4$

FIG. 7. ρ^+ GPD H_3. The same line code is used in Fig. 5.

meson vertex), Ref. [30], etc. (for the cutoff function), different values of the model parameters, m and m_R, are adopted here. Thus, the calculated results are different from theirs. Our calculated value of the magnetic dipole moment, $\mu = 2.06$, is very close to the nonrelativistic value ($\mu = 2$) [70] and to the experimental data. In addition, the estimated mean square radius $\langle r^2 \rangle$ and quadrupole moment Q_ρ in our calculation are also compatible with other calculations. It is

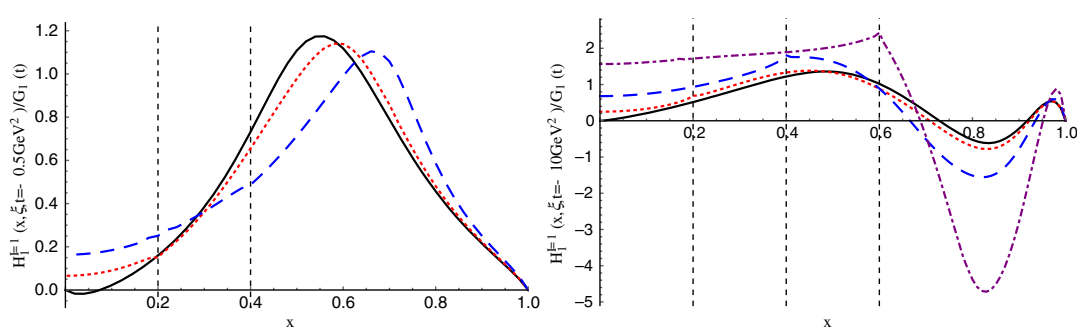

(a) $t = -0.5$ GeV^2, $\xi = 0, -0.2, -0.4$ (b) $t = -10$ GeV^2, $\xi = 0, -0.2, -0.4, -0.6$

FIG. 8. ρ^+ GPD $H_1(x, \xi, t)$ at (a) $t = -0.5$ GeV^2 and -10 GeV^2. The solid black, dotted red and dashed blue curves stand for the H_1 with $\xi = 0, -0.2,$ and -0.4, respectively. The dotted-dashed purple curve in (b) is for $\xi = -0.6$ The vertical dashed lines on the x axis represent $x = |\xi|$.

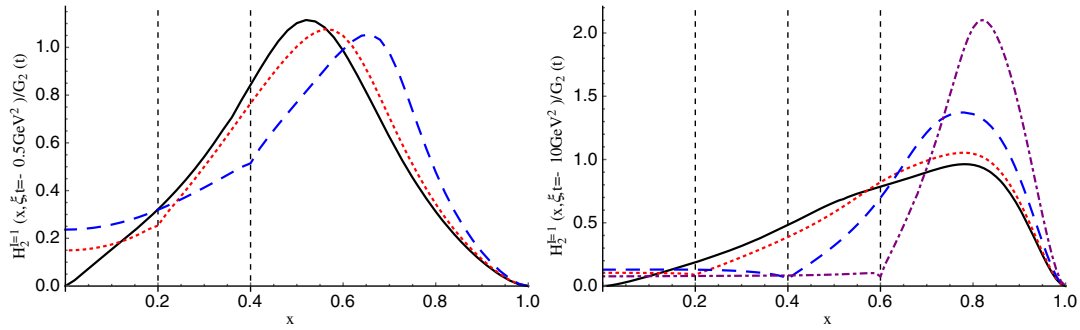

(a) $t = -0.5\ \mathrm{GeV}^2,\ \xi = 0,\ -0.2,\ -0.4$ (b) $t = -10\ \mathrm{GeV}^2,\ \xi = 0,\ -0.2,\ -0.4,\ -0.6$

FIG. 9. ρ^+ GPD H_2. The same line code is used in Fig. 8.

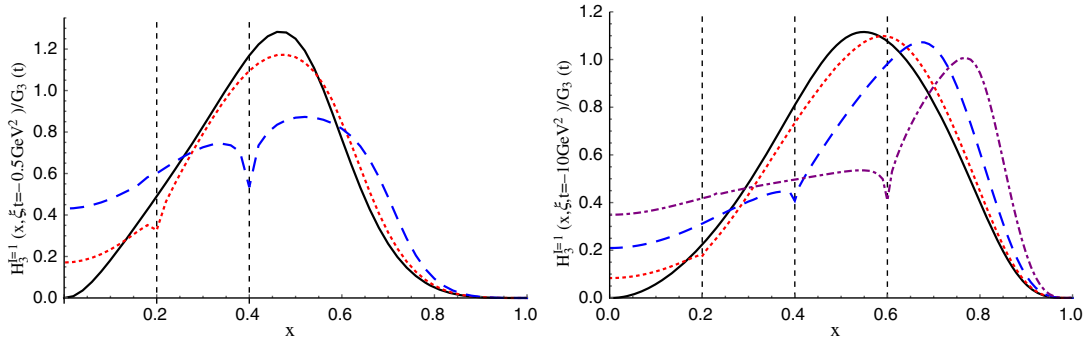

(a) $t = -0.5\ \mathrm{GeV}^2,\ \xi = 0,\ -0.2,\ -0.4$ (b) $t = -10\ \mathrm{GeV}^2,\ \xi = 0,\ -0.2,\ -0.4,\ -0.6$

FIG. 10. ρ^+ GPD H_3. The same line code is used in Fig. 8.

expected that the future measurements for the ρ meson radius and quadrupole moment may provide a test for different model calculations.

The Lorentz invariance requires that the FFs G_i in Eq (5) are frame independent, since the integration over x removes the influence of different light-cone direction n and therefore the integral remains ξ independent. However, it is still interesting to investigate the nonvalence contribution (at $\xi \neq 0$) to G_i. As one can see from Fig. 4, for all three FFs, the valence contributions are dominant in small skewness $|\xi|$, and the percentage of the nonvalence contributions increases as $|\xi|$ does, which is same as the pion case [17]. As $|t|$ increases, the nonvalence contribution in G_1 increases, while those in G_2 and G_3 go oppositely. Especially for G_2, the decrease is very distinct. It is clearly illustrated in Fig. 9(b) for the GPD H_2 at $t = -10\ \mathrm{GeV}^2$. In contrast, in the pion case [17], the nonvalence contribution to the pion form factor is especially large in the large $|\xi|$ and small $|t|$ region. In all three ρ FFs G_i, we find that the sum of the numerical result of the valence and nonvalence

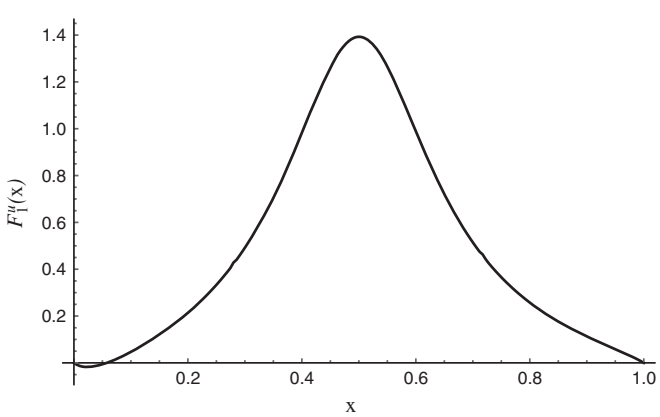

FIG. 11. The DIS structure function F_1^u.

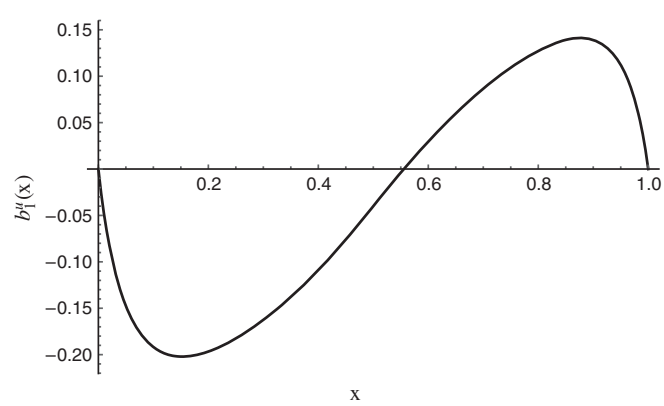

FIG. 12. The DIS structure function b_1^u.

contributions only has negligible variation over ξ. Thus, the frame independence of our model calculation is well satisfied.

It should be stressed that our results, shown in Figs. 5–10, are continuous at $x = \xi$ (or $|\xi|$) as discussed earlier. The ξ trajectory limits that $-0.42 \leq \xi \leq 0$ for $t = -0.5$ GeV^2, and $-0.90 \leq \xi \leq 0$ for $t = -10$ GeV^2. As one can see from Figs. 8(a) and 9(a), in the small $|t|$ region, the transition from the valence to novalence regimes in H_1 and H_2 is quite smooth. However, in the large $|t|$ region, as shown in Figs. 8(a) and 9(b), both H_1 and H_2 become sensitive to the transition in the nonzero skewness case, while Figs. 10 and 7 show that H_3 is very sensitive when $x \to \xi$ (or $|\xi|$) as $\xi \neq 0$, in both the small and large $|t|$ regions.

We know that, in the forward limit ($t \to 0$) and in the deep inelastic region, $H_1^q(x,0,0)/2$ corresponds to the single flavor structure function $F_1^q(x)$ and $H_5^q(x,0,0)$ corresponds to the structure function $b_1^q(x)$. The two obtained functions F_1^u and b_1^u are plotted in Figs. 11 and 12, respectively. Our result for F_1^u has a crossing near $x = 0$, which is beyond the expectation, since as $x \to 0, F_1^u$ should decrease to zero smoothly. This may be due to the fact that the contribution of the gluon GPDs becomes more important in the small-x regime [2], which is beyond the scope of the present calculation. As for $b_1^u(x)$ or more general $H_5^u(x,\xi,t)$, the sum rules Eq. (6) requires the integral over x vanishes for any ξ and t. Our numerical result holds the sum rule for H_4^u quiet well, but for H_5^u, the integral deviates from zero by, at most, ~6.5% [with respect to $G_C(0) = 1$] when -7 GeV$^2 \leq t \leq 0$. The violation of sum rules of H_4 and H_5 is also encountered in the deuteron case, such as the numerical model in Ref. [25]. In addition, the symmetry around $x \sim 1/2$ preserves approximately for both $F_1^u(x)$ and $b_1^u(x)$ in our phenomenological model calculation. This symmetry conforms to the isospin and crossing symmetries, which reduces $u_{\rho^+}(x) = \bar{d}_{\rho^+}(1-x)$.

V. QCD EVOLUTION

It is known that the low-energy chiral quark model provides the initial conditions for the QCD evolution. The present work assumes that the valence quarks carry all the momentum at a factorization scale Q_0. To compare our result with the lattice calculation, the evolution is needed. As far as we know, Ref. [47] is the only one lattice QCD calculation for the moments of the unpolarized ρ meson, which is at the scale $Q = 2.4$ GeV with quenched approximation. Its results are supported by the latter QCD sum rule calculation in Ref. [48]. The leading order (LO) DGLAP evolution for the moments of the single flavor structure function $F_1^u(x)$ reads

$$\frac{V_n^u(Q)}{V_n^u(Q_0)} = \left(\frac{\alpha(Q)}{\alpha(Q_0)}\right)^{\gamma_n^{(0)}/(2\beta_0)}, \tag{40}$$

where the valence-quark momentum fractions $V_n^u = M_{n+1}[H_1^u(x,0,0)] = 2M_{n+1}[F_1^u(x)] \sim a_{n+1}$ and the running coupling constant is

$$\alpha(Q) = \frac{4\pi}{\beta_0 \log(Q^2/\Lambda_{\rm QCD}^2)}, \tag{41}$$

where $\beta_0 = 11N_c/3 - 2N_f/3$ with $N_c = N_f = 3$ and

$$\Lambda_{\rm QCD} = 0.226 \text{ GeV} \tag{42}$$

being employed [29,63]. The percentage of the ρ total momentum carried by the valence quarks is $V_1 = V_1^u + V_1^{\bar{d}}$. In Ref. [47], it was found that $V_1^q(Q = 2.4 \text{ GeV}) = 0.33(2)$ and therefore V_1 is about 70%. At the quark model point Q_0, i.e. the model factorization scale, $V_1(Q_0)$ turns out to be

$$V_1(Q_0) = 1, \qquad G_1(Q_0) + S_1(Q_0) = 0, \tag{43}$$

from the downward LO DGLAP evolution. In the above equation, $G_1(Q)$ and $S_1(Q)$ are the gluon and sea momentum fractions, respectively. Thus, quark model point Q_0 is

$$Q_0 = 528^{+77}_{-62}\text{MeV}. \tag{44}$$

The error bars come from the uncertainty in lattice result for V_1^q. This is a rather low scale; however, the typical expansion parameter $\alpha(Q_0)/(2\pi) = 0.131^{+0.018}_{-0.023}$ makes the perturbation theory meaningful. It should be mentioned that our numerical result for V_1 is 1.02, which diverges from unity by 2%. At the scale $Q = 2.4$ GeV, the results for $V_{1,2,3}$ (or $a_{2,3,4}$) and $d_{2,3,4}$ of Ref. [47] are

$$V_1^u = 0.33(2), \qquad V_2^u = 0.17(5), \qquad V_3^u = 0.06(4), \tag{45}$$

$$d_2 = 0.29^{+22}_{-23}, \qquad d_3 = -0.001(15), \qquad d_4 = -0.01(6). \tag{46}$$

After the LO DGLAP evolution to the lattice scale, our model predicts

$$V_1^u = 0.34(2), \qquad V_2^u = 0.15(1), \qquad V_3^u = 0.08(1), \tag{47}$$

$$d_2 = 0.044(3), \qquad d_3 = 0.048(5), \qquad d_4 = 0.039(5), \tag{48}$$

where the error bars came from the uncertainty of the predicted scale Q_0 in Eq. (44). As one can see, except for d_2, the lowest moments of $b_1^q(x)$, our results agree well with the lattice calculations. However, it should be emphasized

that Ref. [47] concluded their d_2 value being "surprisingly" large at the scale of $Q = 2.4$ GeV, since $b_1^q(x)$ should vanish if the ρ meson is in a pure $^3S_1$ state. We believe that our estimated smaller value for d_2 is more reasonable since only the $^3S_1$-wave coupling is taken into account in the present calculation and the $^3D_1$ admixture is thought to be small ($\sim$1%) as mentioned earlier.

VI. SUMMARY AND CONCLUSIONS

In the present work, we perform a calculation for the ρ meson unpolarized GPDs by employing a light-cone constituent quark model and using the isospin combination [29,63]. The smeared $\rho - q\bar{q}$ meson vertex, which represents the nonperturbative QCD effect, is adopted following Ref. [42] but using the symmetric loop momentum convention in order to satisfy the isospin symmetry. The three ρ meson FFs and some other low-energy observables are calculated. Our results are compatible with the previous calculations. By considering the sum rules of GPDs, the unpolarized DIS structure functions have also been estimated, and the symmetric distribution is basically maintained in our numerical calculation. This feature reflects the isospin and crossing symmetries. At $x = \xi$ (or $|\xi|$) where the DGLAP and ERBL regimes meet, GPDs in our calculation are continuous, as required by the consistency of factorization at leading twist [2]. After the QCD evolution, the model predictions for the moments of structure functions are compared with the lattice calculation. The obtained factorization scale Q_0 is a rather low one in this work. However, the corresponding typical expansion parameter is still small enough to make the perturbative calculation meaningful. It is encouraging that all the first three-order moments in our calculation are compatible with the lattice calculation at the same scale ratio. The present model can be also applied for the polarized GPDs of the ρ meson, and such a calculation is in a progress. Moreover, a calculation for the deuteron GPDs is also expected in the future.

ACKNOWLEDGMENTS

We would like to thank Yu Jia, Wei Sun, Yu Lu, and B. Pire for their useful and constructive discussions. This work is supported by the National Natural Sciences Foundations of China under Grants No. 11475192 and No. 11521505 and by the fund provided to the Sino-German CRC 110 "Symmetries and the Emergence of Structure in QCD" project by NSFC under Grant No. 11621131001.

APPENDIX EXTRACTING THE UNPOLARIZED GPDs

The following is the method to extract the unpolarized GPDs H_i. First, the loop integral, Eq. (29), after excluding the two polarization vectors ϵ_μ and ϵ'^*_ν, is

$$\begin{aligned}
V^{u;\mu\nu}(x,\xi,t) &= \frac{M^2}{f_\rho^2}\frac{1}{2(2\pi)^3\sqrt{\omega_{p'}\omega_p}}\int\frac{d^4k}{(2\pi)^4}\delta[xP^+ - k^+] \\
&\quad\times(-)\mathrm{Tr}\left\{\frac{\imath(\not{k}-\not{P}+m)}{(k-P)^2-m^2+\imath\epsilon}\gamma^\nu\frac{\imath(\not{k}+\frac{\not{\Delta}}{2}+m)}{(k+\frac{\Delta}{2})^2-m^2+\imath\epsilon}\not{n}\frac{\imath(\not{k}-\frac{\not{\Delta}}{2}+m)}{(k-\frac{\Delta}{2})^2-m^2+\imath\epsilon}\gamma^\mu\right\} \\
&\quad\times\frac{c}{[(k-P)^2-m_R^2+\imath\epsilon][(k+\frac{\Delta}{2})^2-m_R^2+\imath\epsilon]}\times\frac{c}{[(k-P)^2-m_R^2+\imath\epsilon][(k-\frac{\Delta}{2})^2-m_R^2+\imath\epsilon]} \\
&= -g^{\mu\nu}H_1^u + \frac{n^\mu P^\nu + P^\mu n^\nu}{n\cdot P}H_2^u - \frac{2P^\mu P^\nu}{M^2}H_3^u + \frac{n^\mu P^\nu - P^\mu n^\nu}{n\cdot P}H_4^u + \left\{\frac{M^2 n^\mu n^\nu}{(n\cdot P)^2} + \frac{1}{3}g^{\mu\nu}\right\}H_5^u.
\end{aligned} \tag{A1}$$

Then, by contracting with the five tensors, one gets five independent equations as

$$\begin{pmatrix} g_{\mu v} \\ n_\mu n_\nu \\ n_\mu P_\nu \\ n_\nu P_\mu \\ P_\mu P_\nu \end{pmatrix}\cdot V^{u;\mu\nu} = \begin{pmatrix} -4 & 2 & -\frac{2P^2}{M^2} & 0 & \frac{4}{3} \\ 0 & 0 & -\frac{2(n\cdot P)^2}{M^2} & 0 & 0 \\ -(n\cdot P) & n\cdot P & -\frac{2(n\cdot P)P^2}{M^2} & -(n\cdot P) & \frac{n\cdot P}{3} \\ -(n\cdot P) & n\cdot P & -\frac{2(n\cdot P)P^2}{M^2} & n\cdot P & \frac{n\cdot P}{3} \\ -P^2 & 2P^2 & -\frac{2P^4}{M^2} & 0 & M^2+\frac{P^2}{3} \end{pmatrix}\cdot\begin{pmatrix} H_1^u \\ H_2^u \\ H_3^u \\ H_4^u \\ H_5^u \end{pmatrix}. \tag{A2}$$

Finally, the explicit expressions for GPDs are obtained:

$$\begin{pmatrix} H_1^u \\ H_2^u \\ H_3^u \\ H_4^u \\ H_5^u \end{pmatrix} = \begin{pmatrix} \frac{1}{6}\left(\frac{P^2}{M^2}-3\right) & \frac{P^2(P^2-M^2)}{2M^2(n\cdot P)^2} & \frac{M^2-P^2}{2M^2(n\cdot P)} & \frac{M^2-P^2}{2M^2(n\cdot P)} & \frac{1}{3M^2} \\ -\frac{1}{2} & -\frac{3P^2}{2(n\cdot P)^2} & \frac{1}{n\cdot P} & \frac{1}{n\cdot P} & 0 \\ 0 & -\frac{M^2}{2(n\cdot P)^2} & 0 & 0 & 0 \\ 0 & 0 & -\frac{1}{2(n\cdot P)} & \frac{1}{2(n\cdot P)} & 0 \\ \frac{P^2}{2M^2} & \frac{3P^4}{2M^2(n\cdot P)^2} & -\frac{3P^2}{2M^2(n\cdot P)} & -\frac{3P^2}{2M^2(n\cdot P)} & \frac{1}{M^2} \end{pmatrix} \cdot \begin{pmatrix} g_{\mu\nu} \\ n_\mu n_\nu \\ n_\mu P_\nu \\ n_\nu P_\mu \\ P_\mu P_\nu \end{pmatrix} \cdot V^{u;\mu\nu}. \tag{A3}$$

[1] H. Marukyan, Int. J. Mod. Phys. A **30**, 1530057 (2015).
[2] M. Diehl, Phys. Rep. **388**, 41 (2003).
[3] C.-R. Ji, Y. Mishchenko, and A. Radyushkin, Phys. Rev. D **73**, 114013 (2006).
[4] K. Kumericki, S. Liuti, and H. Moutarde, Eur. Phys. J. A **52**, 157 (2016).
[5] K. Goeke, M. V. Polyakov, and M. Vanderhaeghen, Prog. Part. Nucl. Phys. **47**, 401 (2001).
[6] C. A. Aidala, S. D. Bass, D. Hasch, and G. K. Mallot, Rev. Mod. Phys. **85**, 655 (2013).
[7] A. Airapetian *et al.*, Eur. Phys. J. C **77**, 378 (2017).
[8] A. Kirchner and D. Muller, Eur. Phys. J. C **32**, 347 (2003).
[9] M. Guidal, M. V. Polyakov, A. V. Radyushkin, and M. Vanderhaeghen, Phys. Rev. D **72**, 054013 (2005).
[10] M. Diehl and P. Kroll, Eur. Phys. J. C **73**, 2397 (2013).
[11] O. V. Selyugin, Phys. Rev. D **91**, 113003 (2015).
[12] N. Sharma, Eur. Phys. J. A **52**, 338 (2016).
[13] Y.-W. Zhang, Phys. Rev. Lett. **115**, 172502 (2015).
[14] P. Hoodbhoy, X. Ji, and W. Lu, Phys. Rev. D **59**, 014013 (1998).
[15] X. Ji, F. Yuan, and Y. Zhao, Phys. Rev. Lett. **118**, 192004 (2017).
[16] W. Broniowski, A. E. Dorokhov, and E. Ruiz Arriola, Few Body Syst. **52**, 295 (2012).
[17] H.-M. Choi, C.-R. Ji, and L. S. Kisslinger, Phys. Rev. D **64**, 093006 (2001).
[18] C. Fanelli, E. Pace, G. Romanelli, G. Salmè, and M. Salmistraro, Eur. Phys. J. C **76**, 253 (2016).
[19] C. Mezrag, H. Moutarde, and J. Rodriguez-Quintero, Few Body Syst. **57**, 729 (2016).
[20] P. Kroll, Eur. Phys. J. A **53**, 130 (2017).
[21] B. Pire, L. Szymanowski, and J. Wagner, Phys. Rev. D **79**, 014010 (2009).
[22] M. Rinaldi, Phys. Lett. B **771**, 563 (2017).
[23] M. Rinaldi and S. Scopetta, Phys. Rev. C **87**, 035208 (2013).
[24] E. R. Berger, F. Cano, M. Diehl, and B. Pire, Phys. Rev. Lett. **87**, 142302 (2001).
[25] F. Cano and B. Pire, Eur. Phys. J. A **19**, 423 (2004).
[26] Y.-B. Dong and C.-Y. Liang, J. Phys. G **40**, 025001 (2013).
[27] C. Mondal, D. Chakrabarti, and X. Zhao, Eur. Phys. J. A **53**, 106 (2017).
[28] W. Broniowski and E. R. Arriola, Phys. Lett. B **574**, 57 (2003).
[29] W. Broniowski and E. R. Arriola, Phys. Rev. D **78**, 094011 (2008).
[30] T. Frederico, E. Pace, B. Pasquini, and G. Salme, Phys. Rev. D **80**, 054021 (2009).
[31] S. J. Brodsky, H.-C. Pauli, and S. S. Pinsky, Phys. Rep. **301**, 299 (1998).
[32] S. Dalley, Phys. Lett. B **570**, 191 (2003).
[33] P. Hagler, Phys. Rep. **490**, 49 (2010).
[34] W. Cosyn and M. Sargsian, arXiv:1704.06117.
[35] Y.-B. Dong, A. Faessler, T. Gutsche, and V. E. Lyubovitskij, Phys. Rev. C **78**, 035205 (2008).
[36] C.-Y. Liang and Y.-B. Dong, Chin. Phys. C **39**, 104104 (2015).
[37] A. Airapetian *et al.*, Nucl. Phys. **B829**, 1 (2010).
[38] L. Y. Glozman, C. B. Lang, and M. Limmer, Phys. Lett. B **705**, 129 (2011).
[39] J. P. B. C. de Melo and T. Frederico, Phys. Rev. C **55**, 2043 (1997).
[40] F. Cardarelli, I. L. Grach, I. M. Narodetskii, G. Salmè, and S. Simula, Phys. Lett. B **349**, 393 (1995).
[41] T. M. Aliev and M. Savci, Phys. Rev. D **70**, 094007 (2004).
[42] H.-M. Choi and C.-R. Ji, Phys. Rev. D **70**, 053015 (2004).
[43] E. P. Biernat and W. Schweiger, Phys. Rev. C **89**, 055205 (2014).
[44] J. P. B. C. de Melo, C.-R. Ji, and T. Frederico, Phys. Lett. B **763**, 87 (2016).
[45] A. F. Krutov, R. G. Polezhaev, and V. E. Troitsky, Phys. Rev. D **93**, 036007 (2016).
[46] J. He, B. Julia-Diaz, and Y.-B. Dong, Phys. Lett. B **602**, 212 (2004).
[47] C. Best, M. Gockeler, R. Horsley, E.-M. Ilgenfritz, H. Perlt, P. E. L. Rakow, A. Schafer, G. Schierholz, A. Schiller, and S. Schramm, Phys. Rev. D **56**, 2743 (1997).
[48] A. Oganesian and A. Samsonov, J. High Energy Phys. 09 (2001) 002.
[49] M. Diehl, T. Gousset, B. Pire, and O. Teryaev, Phys. Rev. Lett. **81**, 1782 (1998).
[50] I. V. Anikin, B. Pire, and O. V. Teryaev, Phys. Lett. B **626**, 86 (2005).
[51] O. V. Teryaev, Phys. Lett. B **510**, 125 (2001).

[52] L. Mankiewicz, G. Piller, and T. Weigl, Eur. Phys. J. C **5**, 119 (1998).
[53] S. A. Morrow *et al.*, Eur. Phys. J. A **39**, 5 (2009).
[54] I. V. Anikin, B. Pire, and O. V. Teryaev, Phys. Rev. D **69**, 014018 (2004).
[55] D. Boer *et al.*, arXiv:1108.1713.
[56] A. Accardi, V. Guzey, C. Weiss, and A. Prokudin, Eur. Phys. J. A **48**, 92 (2012).
[57] X. Ji, Phys. Rev. Lett. **78**, 610 (1997).
[58] F. E. Close and S. Kumano, Phys. Rev. D **42**, 2377 (1990).
[59] W. Cosyn, Y.-B. Dong, S. Kumano, and M. Sargsian, Phys. Rev. D **95**, 074036 (2017).
[60] Y. Dong and C. Liang, Int. J. Mod. Phys. Conf. Ser. **29**, 1460229 (2014).
[61] S. Kumano, Phys. Rev. D **82**, 017501 (2010).
[62] H. Khan and P. Hoodbhoy, Phys. Rev. C **44**, 1219 (1991).
[63] W. Broniowski, E. R. Arriola, and K. Golec-Biernat, Phys. Rev. D **77**, 034023 (2008).
[64] T. Frederico and G. A. Miller, Phys. Rev. D **45**, 4207 (1992).
[65] J. P. B. C. de Melo, T. Frederico, E. Pace, and G. Salme, Nucl. Phys. **A707**, 399 (2002).
[66] F. M. Lev, E. Pace, and G. Salme, Nucl. Phys. **A641**, 229 (1998).
[67] M. Burkardt, Phys. Rev. D **62**, 094003 (2000).
[68] S. J. Brodsky, D. S. Hwang, B. Q. Ma, and I. Schmidt, Nucl. Phys. **B593**, 311 (2001).
[69] M. Diehl, T. Feldmann, R. Jakob, and P. Kroll, Nucl. Phys. **B596**, 33 (2001).
[70] W. Jaus, Phys. Rev. D **67**, 094010 (2003).
[71] B.-D. Sun and Y.-B. Dong, Chin. Phys. C **41**, 013102 (2017).
[72] G. A. Miller, Phys. Rev. C **80**, 045210 (2009).
[73] C. S. Mello, A. N. da Silva, J. P. B. C. de Melo, and T. Frederico, Few Body Syst. **56**, 509 (2015).
[74] B. J. Owen, W. Kamleh, D. B. Leinweber, M. S. Mahbub, and B. J. Menadue, Phys. Rev. D **91**, 074503 (2015).
[75] D. G. Gudino and G. T. Sanchez, Int. J. Mod. Phys. Conf. Ser. **35**, 1460463 (2014).